Quantifying Joint Congruence with an Elastic Foundation

Charles B. Burson-Thomas*
Research Fellow

Alexander S. Dickinson
Associate Professor in Mechanical Engineering

Martin Browne
Professor of Applied Biomaterials

Bioengineering Sciences Research Group
Department of Mechanical Engineering
University of Southampton
UK
Email: c.b.burson-thomas@soton.ac.uk

The level of congruence between the articulating surfaces of a diarthrodial joint can vary substantially between individuals. Quantifying joint congruence using the most widespread metric, the 'congruence index', is not straightforward: the areas of the segmented bone that constitute the articular surfaces require accurate identification, their shape must be carefully described with appropriate functions, and the relative orientation of the surfaces measured precisely. In this work, we propose a new method of measuring joint congruence, which does not require these steps. First, a Finite Element (FE) simulation of an elastic layer compressed between each set of segmented bones is performed. These are then interpreted using the elastic foundation model, enabling an equivalent, but simpler, contact geometry to be identified. From this, the equivalent radius (quantification of joint congruence) is found. This defines the radius of a sphere contacting plane (or 'ball on flat') that produces an equivalent contact to that in each joint. The minimal joint space width (in this joint position) can also be estimated from the FE simulations. The new method has been applied to 10 healthy instances of the thumb metacarpophalangeal (MCP) joint. The ten thumb MCPs had similar levels and variability of congruence as the other diarthrodial joints that have been characterised previously. This new methodology enables efficient quantification of joint congruence and minimal joint space width directly from CT or MRI derived bone geometry in any relative orientation. It lends itself to large data sets and coupling with kinematic models.

*Please address all correspondence to this author.

1 Introduction

Two surfaces are congruent if they are identical in both size and shape [1]. Given that mechanical stress is strongly implicated in the development of osteoarthritis [2] and that higher contact stresses have been shown to be a strong indicator of the potential to develop symptomatic osteoarthritis [3], one might initially consider two congruent articular surfaces to be the 'ideal' geometry for a diarthrodial joint. In theory, this would maximise the area over which the load is transmitted, reducing both the peak stress and the average stress experienced by the articular cartilage. However, there are also a number of benefits to the geometry of the articular surfaces being less than perfectly conforming. Firstly, it does not necessarily follow that the stress distribution generated by two congruent surfaces in contact is ideal mechanically: at the edges of the contact area, a larger discontinuity in stress would be generated in the articular cartilage than where there is some incongruence. Incongruence also benefits joint lubrication. M.A. MacConaill was the first [4] to propose the incongruency of the articular surfaces generates a hydrodynamic mode of lubrication [5], offering one explanation for why diarthrodial joints are able to exhibit such low coefficients of friction. MacConaill's theory of joint lubrication has now been superseded, with several modes of lubrication now considered to be active in diarthrodial joints and hydrodynamic lubrication playing a supportive, rather than dominant, role [6]. However, a form of hydrodynamic lubrication, particularly when joints are experiencing high speed and low loads, is likely to be active in diarthrodial joints [6]. There are also implications for joint kinematics and permissible anatomical shape. Requiring two perfectly-conforming

articular surfaces is much more constraining than permitting some incongruence. The articular surfaces of diarthrodial joints do not only slide but roll with respect to each other [7]. Rolling is not feasible if the two surfaces are to be congruent in all positions. In practice, diarthrodial joints exploit the freedom permitted by incongruent surfaces to enable complex and unique kinematics [8]. Putting the advantages and disadvantages of congruent articular surfaces to one side, perhaps the source of the greatest interest in joint congruence is exposed: different people have quite different levels of congruence in their joints. Why is this? Is there a level of congruence that is optimal? Do some levels of congruence make people more at risk of developing osteoarthritis? In order to engage with these questions, one must first be able to quantify the level of congruence between the two articular surfaces.

Ateshian *et al.* [9] drew upon the concept of an 'equivalent surface' in their quantification of joint congruence in 13 thumb carpometacarpal joints. When two different surfaces contact, it is possible to define a surface that is in contact with a plane that generates an equivalent contact. This 'equivalent surface' is found from the difference between the two original surfaces [9, 10]. There are several benefits to calculating an equivalent surface. For example, in contact mechanics, this has been exploited for many years to enable different pairs of contacting surfaces to be analysed as a Hertzian contact [10]. It also enables different contact pairs to be more conveniently compared; this is exploited in the quantification of incongruity by Ateshian *et al.* [9]. The equivalent surface can be described in terms of its two principal curvatures, κ^e_{max} and κ^e_{min}. The 'congruence index' or 'CI' proposed by Ateshian *et al.* [9] is found by taking the Root Mean Square (RMS) of the two principal curvatures:

$$CI = \sqrt{\frac{(\kappa^e_{min})^2 + (\kappa^e_{max})^2}{2}}. \quad (1)$$

Thus, it is a measure of the average curvature of the equivalent surface. Two surfaces that are completely congruent would have a CI of zero; the equivalent surface would be a plane. The CI quantification of joint congruence has been employed in several subsequent studies: 46 further thumb carpometacarpal joints [11], 14 human knees [12], and 10 further patellofemoral joints [13]. In more recent years, several alternative quantifications of joint congruence have been proposed; these are summarised in Table 1 [14–17]. In addition, other investigators have sought to quantify congruence via the measurement of associated physical parameters, including subluxation [18] and width of joint space [19].

Whilst there are potential advantages of other quantification methods, the physical clarity and strong basis in geometry of the CI means that this quantification of joint congruence is yet to be supplanted. However, this does not mean that further development of the methodology is unwarranted. When evaluating the CI, the areas of two digital bone geometries (segmented from CT or MRI scans) that are considered to be the two articular surfaces has a substantial influence on the resulting value [13]. In addition, care must be taken with the description of the articular surfaces. For example, when interpolating B-spline functions to describe an articular surface, the curvature generated is dependent on the error allowed between the B-spline and vertices the surface is being fitted to: too small an error and noise is generated; too large an error and relevant information might be lost [12]. Finally, the relative orientation of the articular surfaces must be quantified precisely, particularly if the effect of joint position is to be explored [13, 15].

In this study, we propose an alternative method to quantify joint congruence that employs the concept of an equivalent surface and description of its shape. First, a Finite Element (FE) simulation of an elastic layer compressed between the two bones is performed, where all assumptions are consistent with the elastic foundation model except those concerning bone geometry: in each FE simulation, the surface of the two bones is approximated through discretisation into many triangular faces; in the elastic foundation model, the two bone surfaces are reduced to an elliptic paraboloid and plane. By interpreting the results of the simulation with the elastic foundation model, a parameter that is very closely related to the CI is determined—the 'equivalent radius'. Whereas the CI is a measure of the average curvature of the joint's equivalent surface, the physical meaning of the equivalent radius is perhaps more easily visualised: it defines the radius of a sphere contacting plane (or 'ball on flat') that produces an equivalent contact to that in each participant's joint. In addition, the FE simulation provides an estimate of the minimal joint space width (in this joint position). This new method is demonstrated by quantifying the congruence of 10 thumb metacarpophalangeal (MCP) joints. Focussing on the thumb MCP joint enabled this study to quantify the congruence of a joint with known variation in shape, where the congruence had not previously been characterised.

2 Materials and Methods

2.1 Joint and identification of its geometry

The thumb MCP joint connects the first metacarpal and first proximal phalanx, and is the second most distal joint of the thumb. It is a condyloid joint for which there is 'no precise mechanical equivalent' [21]; experimental measurement of cadaveric hands has suggested there are two non-orthogonal axes of rotation [22]. However, others have described the thumb MCP to have three degrees-of-freedom [8, 21], adding pronation-supination to flexion-extension and abduction-adduction, and suggested it is best approximated as a universal joint [21]. The characteristics of this joint are critical for the prehensile action of the thumb; it provides necessary constraint during several gripping actions [8]. Whilst several studies [9, 11, 15] have quantified the congruence of the joint proximal to the thumb MCP—the thumb carpometacarpal (or trapeziometacarpal) joint—no quantification of joint congruence could be found for the thumb MCP joint. However, the distal end of the first metacarpal bone has been observed to vary substantially in shape between individuals [23]. This variation in shape has implica-

Table 1. Alternative quantifications of joint congruence to the Ateshian *et al.* [9] 'congruence index' (CI)

Study	Summary of proposed quantification of joint congruence
Tummala *et al.* [14]	A 'congruity index' that is evaluated locally, in a piecewise manner, and then averaged over the contact area to give an overall indication for two contacting surfaces. The local congruence quantification is the reciprocal of the distance between the two local normal vectors (one for each contacting surface), which have been scaled by the local normal curvatures. For congruent surfaces the quantification will tend to infinity; the scale bar for 'congruity map' of a healthy medial tibio-femoral joint was set between 0 and 10 [14].
Halilaj *et al.* [15]	A 'positional joint congruence' that is designed to quantify the congruence of two articular surfaces based on both geometry and joint position. First, 3D polar histograms of curvature are constructed of each articular surface, which have been scaled to removed the effect of size. The quantification of congruence is a statistical description of the level of dissimilarity between the two histograms that describe each articular surface, in each joint position. A linear weighting factor was included to ensure that points on the articular surface that are in closer proximity to the other articular surface have a greater influence on the final quantification of congruence.
Conconi and Perenti Castelli [16]	A 'congruence measure' developed using the elastic foundation model [10]. One bone is expanded by a distance $\underline{\Delta}$ in all directions, sufficient that the expanded bone intersects the other bone connected at the joint. The volume of intersection between the expanded bone and the other bone, $\underline{V}$, is calculated. The quantification of congruence is calculated by $\underline{V}/\underline{\Delta}$. This is equal to the force divided by the peak pressure for an elastic layer, if the compressed volume of the layer is $\underline{V}$ and its maximum indentation is $\underline{\Delta}$. The quantification of congruence is a function of $\underline{\Delta}$; thus, the expansion of the bone 'must be kept constant within a group to be sorted' [16]. Later work has sought to address this limitation by proposing a normalisation of the quantity [20].

tions for the joint kinematics: the 'flatter' the distal end of the first metacarpal, the lower the overall range of motion of the thumb MCP; the more 'curved' the distal end, the greater the overall joint range of motion [24, 25].

Ten participants free from hand or wrist disease or injury were recruited for CT imaging as part of a larger study on hand biomechanics (IRAS Ethics Ref: 14/LO/1059) [26]. Participants were sex matched (5 female, 5 male) with mean age of 31 years (range: 27–37 years). Each participant's right hand was CT scanned (Discovery CT750 HD 128 scanner, GE Healthcare Inc., USA) with near-isotropic voxel size (0.293 x 0.293 x 0.312 mm), 1825 ms exposure time, and 0.7 mm spot size. The scans were collected with the hand supported by an adjustable Nylon jig, with the fingers in full extension. CT data were segmented using ScanIP (Synopsys Inc., USA): the outlines of the first metacarpal and first proximal phalanx were identified using a greyscale threshold, the bones were separated using a particle split function, and each assigned a triangular surface mesh. The surface meshes were imported into MATLAB [27], where the bones were aligned to a coordinate system proposed by the International Society of Biomechanics (ISB) [28]. The body segment coordinate system for the first metacarpal was employed for both bones, where: the origin is at the centroid of the first metcarpal; the x-axis points volarly; the y-axis is directed proximally, along the the length of the first metacarpal; and the z-axis points radially. To align each participant's first metacarpal and first proximal phalanx to this coordinate system, a previously-employed [26, 29] two-stage alignment process was used: an initial alignment by Principal Component Analysis (PCA), which was refined by the Iterative Closest Point (ICP) registration approach [30]. More precisely: after translating the bones such that the origin was located at centroid of the metacarpal bone, PCA of the x, y, and z coordinates of the first metacarpal was used to identify an initial rotation to align each bone with the ISB coordinate system. This rotation was refined by selecting one participant, whose bones had been well-aligned by PCA alone, and, using a MATLAB implementation [31] of the ICP registration approach [30], a second finer-rotation for each of the other nine participant's bones was defined and then applied.

2.2 Elastic foundation model

The elastic foundation model is detailed in Johnson's seminal work on contact mechanics [10]. In addition to being referred to as the 'elastic foundation model' [16, 20, 32], this model has also been described as: Winkler elastic foundation [10], Discrete Element Analysis (DEA) [3, 33], rigid-body-spring-model [34], and some version of 'elastic layer on rigid foundation' [35, 36]. Much of its previous use in the field of biomechanics has been in a discretised form [3, 32–35], which requires numerical integration. However, if the geometry of the contacting surfaces is reduced to an elliptic paraboloid and plane, a closed-form solution is available [10]. As will be shown, this closed-form solution can be used to interpret an analogous FE simulation and quantify the joint congruence from the variation of force with maximum compressive strain.

Figure 1 shows the basic assumptions of elastic foundation model: an elastic layer between two rigid surfaces is

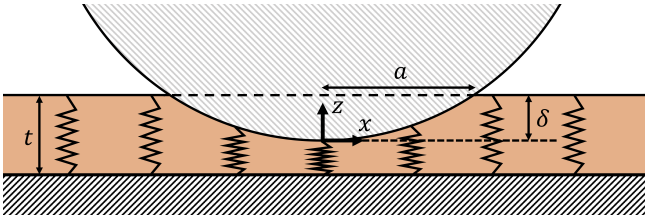

Fig. 1. Elastic foundation model: an elastic layer between two rigid surfaces is modelled as a set of independent springs. A 2D plane is shown (xz-plane). However, the model is 3D, with one surface being a plane and the other described by an elliptic paraboloid. The maximum deformation of elastic layer by the rigid paraboloid, δ, occurs at the origin of the coordinate system. An elliptical contact area is generated, which is described by two semi-axes in the x and y directions. Only one is shown, a, which is the semi-axis in the x direction (b is the semi-axis in the y direction). The initial thickness of the elastic layer is t.

modelled as set of independent springs. The many independent 'springs' that constitute the elastic layer are assumed to have no interaction with each other and behave in a linear-elastic manner, with a constant modulus, E. As the two surfaces that compress the elastic layer are rigid, the difference in their shape defines the deformation of the layer. Thus, like the non-planar surface, the deformation is paraboloidal. The local stress at a point in the contact region can be calculated from the local deformation, and the resulting paraboloidal distribution of stress integrated over the contact area to give the total load, P. Johnson [10] shows how this results in an analytical solution:

$$P = \frac{E\pi ab\delta}{2t}. \tag{2}$$

In addition to being dependent on the modulus of the layer, the load (Eqn. 2) is dependent on: the thickness of the elastic layer, t; the maximum deformation, δ; and the dimensions of the ellipsoidal contact area, a and b (the two semi-axes). It can be shown that $a = (2\delta R')^{1/2}$ and $b = (2\delta R'')^{1/2}$, where R' is the radius of curvature in the xz plane and R'' is the radius of curvature in the yz plane (radii of curvature calculated at the origin). If a and b are substituted for their dependency on R', R'', and δ, the expression becomes

$$P = \frac{E\pi {R'}^{1/2} {R''}^{1/2}\delta^2}{t}. \tag{3}$$

Furthermore, an 'equivalent radius', R_e, can be defined [10],

$$R_e = {R'}^{1/2} {R''}^{1/2}, \tag{4}$$

which is an average of the two radii of curvature, R' and R''. It is noteworthy that R_e is closely related to the Gaussian curvature (K), which is the product of the two principal curvatures (κ_{max} and κ_{min}) [37]:

$$K = \kappa_{max}\kappa_{min} = \frac{1}{R'R''} = \frac{1}{R_e^2}. \tag{5}$$

If Eqn. 3 is rearranged and expressed using R_e, it is clearer to observe that a plot of P/E on the y-axis, against $(\delta/t)^2$ on the x-axis, should produce a straight line through the origin if no geometric changes are made:

$$\frac{P}{E} = \pi R_e t \left(\frac{\delta}{t}\right)^2. \tag{6}$$

This is because the gradient, $\pi R_e t$, is constant for a particular geometry.

If the articular surfaces of a participant's joint can be reduced to a contact pair described by an elliptic paraboloid and plane, when the results of an analogous FE simulation are plotted on a graph of P/E against $(\delta/t)^2$, they should produce a straight line through the origin—only the gradient should vary between the different participant's joints. If this is the case, then the equivalent surface (the difference between the articular surfaces) of the articular contact pair is well-described by an elliptic paraboloid. Furthermore, these equivalent surfaces (one for each joint instance) can be characterised and compared by their equivalent radius (R_e).

2.3 Analogous Finite Element simulations

The FE simulation is 'analogous' as it employs the same assumptions as the elastic foundation model bar one: in the elastic foundation model, the equivalent surface (difference between contact pair) is described by an elliptic paraboloid, whereas in the analogous FE simulation the geometry of the contacting surfaces is approximated via the use of many triangular faces. Two pieces of software were selected to perform the analogous FE simulations: FEBio [38] and GIBBON (Geometry and Image-Based Bioengineering add-ON) [39]. FEBio was selected as it: is open-source; has been developed specifically for biomechanical analysis; and has enjoyed widespread use in the biomechanics research community for several years [40]. GIBBON (which runs in MATLAB [27]) was used as a pre- and post-processor for FEBio. It enabled code-based development of model geometry, boundary conditions, and simulation parameters.

Figure 2 shows the two bones connected at one participant's thumb MCP joint, with an elastic layer between the surfaces of the bones. The dimensions of the elastic layer in each simulation were 20 mm by 20 mm, with a thickness of 0.6 mm. The elastic layer was made large enough that the boundary conditions required to secure it in space were sufficiently far from the contact region to have a negligible influence on the compression. In order to locate the elastic layer between the two bones, a rigid translation was applied to the proximal phalanx of each participant's joint before the

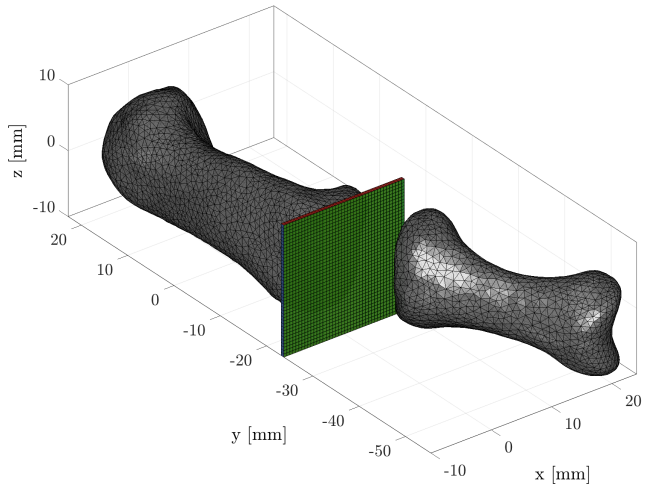

Fig. 2. An example thumb MCP joint geometry. The first proximal phalanx has been translated 6 mm distally (from its anatomical position) to create space for the elastic layer between the surfaces of the bones.

Table 2. Mesh details for elastic layer in each joint geometry

Parameter	Value
Overall dimensions	20 mm by 20 mm by 0.6 mm
Number of elements	1600
Element size	0.5 mm by 0.5 mm by 0.6 mm
Element type	8-node trilinear hexahedral (hex8)

elastic layer was generated: the proximal phalanx was translated 6 mm distally from its anatomical position, along its first principal axis (determined using PCA). In each participant's joint, the two bone surfaces were meshed with 3-node triangular surface elements (tri3) using the vertices identified by the segmentation. Table 2 tabulates the mesh details for the elastic layer in all ten joint geometries. A mesh verification study was performed to ensure the number of elements in the elastic layer was sufficient.

As the two bones were modelled as rigid surfaces, only the elastic layer required constitutive properties. The elastic foundation model assumes a linear-elastic constitutive model, with no lateral expansion due to compression. Thus, the 'isotropic elastic' material model was selected, with 20 MPa used for elastic modulus and a Poisson's ratio of 0. The frictionless contact at each interface, between the elastic layer and bone surfaces, was modelled using the 'sliding-facet-on-facet' algorithm [41]. This algorithm is based on the work of Laursen and Maker [42] and has been developed further to provide additional numerical stability [41]. The FE simulation was performed in displacement-control, which was selected over force-control due to greater numerical stability. In order to compress the elastic layer, the proximal phalanx was translated proximally, along its first principal axis (from PCA)—back towards its anatomical position. Once the elastic layer started to undergo notable compressive strains (of the order 1%), the proximal phalanx was translated in increments of 0.01 mm, with the reaction force (in the direction of translation) generated by the elastic layer recorded. This continued until the maximum deformation of the elastic layer (δ) was 0.15 mm; one quarter of its thickness or maximum compressive strain of 25%. This upper limit on deformation was selected as FEBio's 'isotropic elastic' material model is unsuitable for large strains [41].

To generate appropriate boundary conditions, every node of each metacarpal bone surface was fixed in position (no translation permitted in any direction). In addition, the nodes on the dorsal edge of the elastic layer were also fixed in position. This prevented the elastic layer being under-constrained, without significantly affecting the compression of the elastic layer in the contact region. This was verified through analysing the displacement and strain of the elastic layer, as the proximal phalanx was gradually translated in a proximal direction.

2.4 Identification of equivalent radius and minimal joint space width

In order to quantify the joint congruence from the analogous FE simulations, Eqn. 6 was used. The maximum compressive strain of the elastic layer ($-\varepsilon_{min}$) is equal to the maximum deformation of the elastic layer divided by its thickness (δ/t). Thus, a plot P/E against ε_{min}^2 (like $(\delta/t)^2$, as in Eqn. 6) should produce a straight line through the origin:

$$\frac{P}{E} = (\pi R_e t)\varepsilon_{min}^2. \tag{7}$$

The reaction force (equivalent to total load, P) was recorded for each translation (proximal is positive) of the proximal phalanx from its anatomical position, Δ, in the FE simulation. The maximum compressive strain ($-\varepsilon_{min}$) was calculated from the mean of the five greatest compressive elemental strains within the elastic layer, in the direction of load (the displacement of the proximal phalanx). This value was found to be a good compromise between the need to smooth the numerical instability observed by only using the maximum value of compressive elemental strain, without overly decreasing the value such that it is unrepresentative. Five elements correspond to a contact area of 1.25 mm^2 (see Table 2), given that one can expect metacarpal joint contact areas to be of the order of tens of mm^2 [43], this is still a relatively small area in the context of the joint. MATAB [27] was used to fit linear regressions (with a zero intercept) to a plot of P/E against ε_{min}^2 for each FE simulation (one for each participant's joint), R_e was calculated by dividing the gradient by πt.

The relationship between ε_{min} and Δ was used to estimate the minimal joint space width (mJSW) from the results of the analogous FE simulations. Once the elastic layer starts to be compressed by translation of the proximal phalanx towards the metacarpal, a linear relationship between

ε_{min} and Δ is expected from the elastic foundation model: ε_{min} is given by $-\delta/t$, and Δ is the sum of the displacement from the anatomical position to the start of the elastic layer (Δ_0) and the maximum displacement of the elastic layer (δ):

$$\Delta = \Delta_0 + \delta. \tag{8}$$

Thus, both ε_{min} and Δ are linear functions of δ, and so when plotted against each other should produce a straight line graph. It is Δ_0 that is of interest when calculating the mJSW, as

$$mJSW = \Delta_0 + t. \tag{9}$$

To calculate Δ_0 from a plot of ε_{min} against Δ, consider the value of Δ when ε_{min} is reduced to nothing: when $\varepsilon_{min} = 0$, then $\delta = 0$ ($\varepsilon_{min} = -\delta/t$), thus $\Delta = \Delta_0$ (from Eqn. 8). Therefore, to find Δ_0 for each participant's joint, MATAB [27] was used to fit linear regressions (with an intercept) to each plot of ε_{min} against Δ, and the gradient and intercept used to calculate the intersection with the Δ-axis. Finally, t was added (Eqn. 9) to give the mJSW for each participant's joint.

Finally, in order to investigate the influence of size on the values of R_e and mJSW identified, the length of the first metacarpal was calculated for each participant. This was found by taking the difference between the maximum and minimum y-coordinate in the set of nodes that described the surface of each bone.

3 Results

3.1 Analogous Finite Element simulations

Figure 3 shows the variation of load divided by modulus of elastic layer with maximum compressive strain squared from the ten analogous FE simulations, where an elastic layer was inserted between the segmented bone surfaces of each participant's joint and compressed. The elastic layer response described by the elastic foundation model (Eqn. 7) is strongly represented in all FE simulations: for all ten joint geometries, P/E is well-described as being directly proportional to ε^2_{min}, with only the constant of proportionality (or gradient of the straight line) varying between the participants.

Figure 4 shows the relationships between the displacement (from anatomical position) of the proximal phalanx, Δ, with ε_{min}. An initial non-linear response between Δ and ε_{min} was observed. However, after the maximum compressive strain of the elastic layer had exceeded 5%, all analogous FE simulations suggested the relationship between Δ and ε_{min} could be well-described as linear—as suggested by the elastic foundation model.

Figure 5 shows how the compressed area of the elastic layer (A) varied for each joint geometry, as the maximum compressive strain ($-\varepsilon_{min}$) increased. The maximum compressed area—defined by the number of elements experiencing compressive strains of 1% or greater—varied between

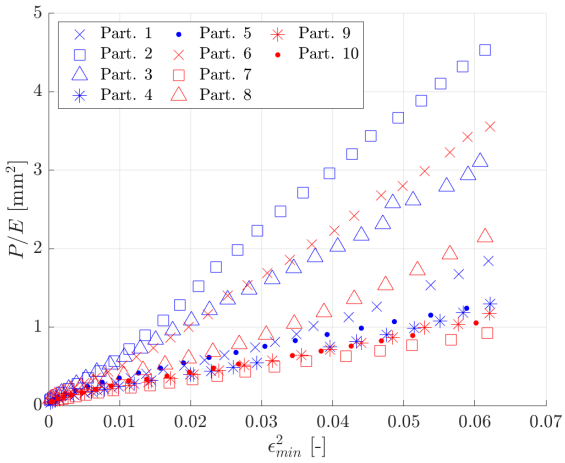

Fig. 3. Analogous FE simulation results of elastic layer response for all ten participants. Axes selected for calculation of equivalent radius: the relationship between load divided by modulus of elastic layer (P/E) and maximum compressive strain squared (ε^2_{min}).

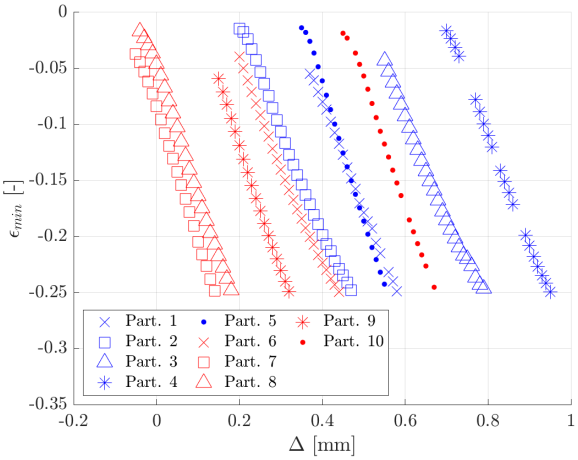

Fig. 4. Analogous FE simulation results of elastic layer response for all ten participants. Axes selected for estimation of minimal joint space width: the relationship between maximum compressive strain of the elastic layer ($-\varepsilon_{min}$) and displacement of the proximal phalanx (Δ). Some of the simulations were unable to converge, as shown in the gaps between the usual 0.01 mm increments in Δ: this is particularly evident for Participant 4.

participants. However, between the minimum and maximum values of $-\varepsilon_{min}$ (0.01–0.25), all joint geometries showed changes in A from single to double digit values of mm^2.

3.2 Equivalent radii and minimal joint space widths

Table 3 shows the equivalent radius and minimal joint space width of each participant's thumb MCP joint (in one joint position). These were identified from the results of the analogous FE simulations shown in Fig. 3 and Fig. 4. In order to avoid the initial non-linear response from some analo-

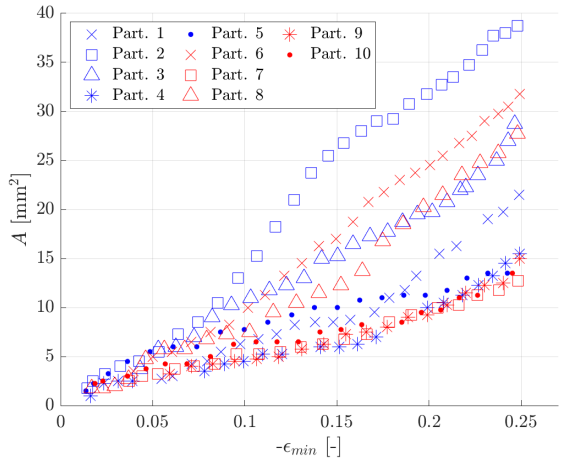

Fig. 5. Variation in compressed area (A) with maximum compressive strain ($-\varepsilon_{min}$) for analogous FE simulation results of elastic layer response, for all ten participants. A was calculated from the number of elements experiencing compressive strains of 1% or more (in the direction of the load).

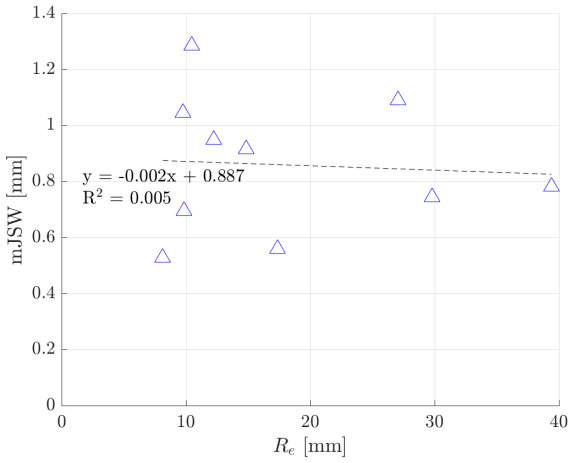

Fig. 6. Relationship between minimal joint space width (mJSW) and equivalent radius (R_e).

Table 3. Equivalent radius (R_e) and minimal joint space width (mJSW) of each participant's thumb MCP joint (in one joint position), determined from results of analogous FE simulations

Participant	R_e (mm)	mJSW (mm)
1	14.8	0.92
2	39.4	0.78
3	27.0	1.09
4	10.5	1.29
5	12.2	0.95
6	29.8	0.74
7	8.1	0.53
8	17.4	0.56
9	9.8	0.70
10	9.8	1.05
Mean	17.9	0.86
Standard deviation	10.6	0.24

gous FE simulations influencing the mJSW estimation, only points where the maximum compressive strain of the elastic layer had exceeded 5% were used in the calculation.

Figure 6 shows the relationship between equivalent radius and minimal joint space width for the ten thumb MCP joints investigated. There was no apparent correlation between the two.

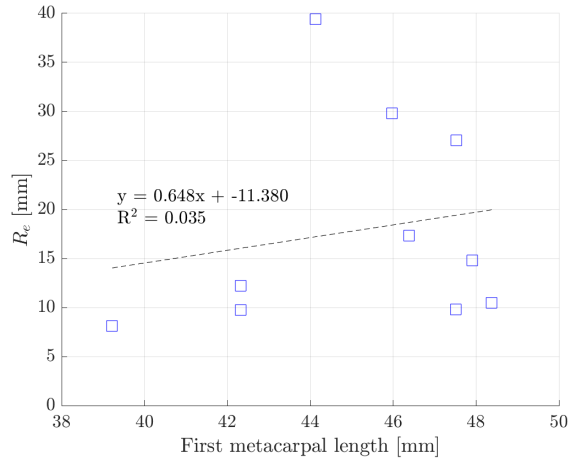

Fig. 7. Effect of bone size on equivalent radius (R_e)

3.3 Effect of bone size

Very weak correlations were observed between bone length and R_e, and bone length and mJSW, for the 10 participants (Figs. 7 and 8).

4 Discussion

An alternative method to quantify joint congruence was applied to ten thumb MCP joints. This new method finds the equivalent radius of the equivalent surface of each contact pair. It does this via an FE simulation of an elastic layer compressed between the bones, which is then interpreted using the elastic foundation model.

4.1 An equivalent surface described by an elliptic paraboloid

The elastic foundation model is derived for an elastic layer compressed between an elliptic paraboloid and a plane.

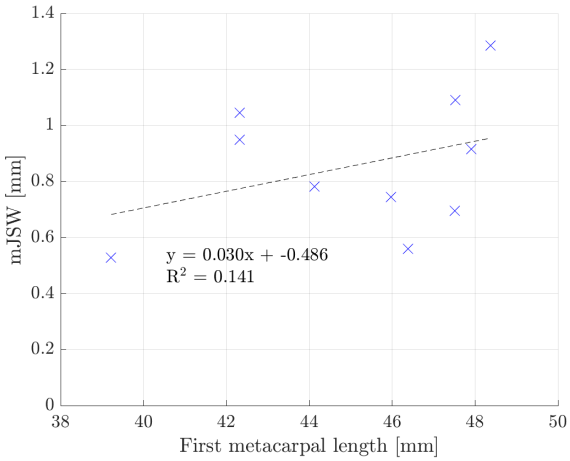

Fig. 8. Effect of bone size on minimal joint space width (mJSW).

The analogous FE simulations removed this restriction on geometry by approximating the shape of the articular surfaces via the use of many triangular faces. This enabled the assumption of an equivalent surface described by an elliptic paraboloid to be tested. The analogous FE simulations indicated little deviation from the expectations of the elastic foundation model; the relationships between P/E and ε_{min}^2 (Fig. 3), and Δ and ε_{min} (Fig. 4), were well-described as linear. Some initial non-linearity was observed in the plots of Δ against ε_{min}. However, this is to be expected at the start of the compression of the elastic layer in the FE simulation. Initially, some nodes in the contact region will not be acted upon by the contact algorithm, due to the approximation of the shape by discretising into many faces. The non-linear behaviour soon abated, once maximum compressive strains of 5% were reached. In addition, whilst there was variation in the maximum compressed area of the elastic layer in the analogous FE simulations, all were of the order of tens of mm^2 (Fig. 5). These constitute a substantial percentage of typical metacarpal joint contact areas, which are unlikely to exceed much more than 100 mm^2 (even in strong grasps) [43]. Given that the lowest value of A was close to 1 mm^2 (ε_{min} mean of five elements, covering an area of 1.25 mm^2), the assumption of an equivalent surface described by an elliptic paraboloid was also consistent over a range of joint areas.

The consistency between the elastic foundation model and analogous FE simulations suggests that the equivalent surface of each participant's thumb MCP joint was well-approximated by an elliptic paraboloid. This has implications beyond supporting the alternative methodology described in this work for quantifying joint congruence. The selection of an elliptic paraboloid to describe the non-planar surface in the elastic foundation model is deliberate; this surface description is far more convenient mathematically than many alternatives, and enables closed-form (analytical) solutions to be found. The demonstration in this work of how successfully an elliptic paraboloid can approximate the equivalent surface of ten examples of a diarthrodial joint suggests that further application and development of analytical contact mechanics [10] may still be appropriate for modelling joints, despite the advances made in recent FE studies.

4.2 Comparison with congruence index

The equivalent radius is closely related to the CI (Eqn. 1), yet they are not equivalent. The equivalent radius is an average of the equivalent surface's two principal radii (R' and R''), whereas the CI is a different average of its two principal curvatures (κ_{max}^e and κ_{min}^e). Therefore, there is actually only one difference between the CI and R_e, other than the choice of physical parameter (curvature or radius): the method of averaging. When calculating R_e, the geometric mean [1] is used to average the two principal radii, instead of finding the RMS of the two (as with the CI). Ateshian *et al.* [9] justify their choice of averaging using the RMS over the geometric mean (which would be $(\kappa_{min}\kappa_{max})^{1/2}$) by describing the consequence of a principal curvature of zero. If $\kappa_{min} = 0$ then the geometric mean would be zero, even if $\kappa_{max} \neq 0$. However, in this new methodology for quantifying joint congruence, this potential issue is avoided: the R_e is found directly from the plot of P/E and ε_{min}^2, and not from the combination of R' and R''.

Unfortunately, for the purposes of direct comparison, the difference between the two methods of averaging (RMS for the CI, geometric mean for R_e) is not negligible, when typical values [9] of κ_{max}^e and κ_{min}^e are considered: $\sqrt{(0.085^2+0.12^2)/2} = 0.104$; $\sqrt{0.085 \cdot 0.12} = 0.101$. Yet, the difference between the two methods of averaging is not so large that an approximation of the CI can not be found from R_e. Thus, an estimate for the CI can be found from the reciprocal of the equivalent radius:

$$CI \approx \frac{1}{R_e}. \tag{10}$$

The geometric mean is always less than the RMS [44]. Thus, the estimate of CI using Eqn. 10 will always be an underestimate.

The mean of the ten ${R_e}^{-1}$ values for the thumb MCP joint was 0.073 mm^{-1}, standard deviation 0.034 mm^{-1}. This is similar to previous quantifications of the CI [9, 11, 12], as shown in Table 4. This comparison with previous work suggests the ten thumb MCPs were towards the less-incongruent end (lower mean CI, thus larger R_e) of previous quantifications of joint congruence. It is true that the systematic underestimation of CI, though using Eqn. 10, will have also assisted in reducing the mean value. However, the effect of this is not expected to be so large that the general conclusion is altered.

4.3 Congruence and minimal joint space width of thumb metacarpophalangeal joint

Both the R_e and mJSW of the thumb MCP joint varied considerably between the 10 participants: R_e ranged from

Table 4. Comparison of estimated CI (from R_e identified) with CI values from previous studies

Joints	Mean CI (mm^{-1})	Standard deviation (mm^{-1})
10 thumb MCPs (this study)	0.073*	0.034*
12 thumb carpometacarpals [9]	0.104	0.044
18 'middle-aged' (40–59 years) thumb carpometacarpals [11]	0.092	0.031
28 'elderly' (60–79 years) thumb carpometacarpals [11]	0.073	0.033
12 femoro-patellars [12]	0.080	0.007
12 medial femoro-tibials [12]	0.069	0.019
12 lateral femoro-tibials [12]	0.069	0.011

*Estimated from R_e

8.1 mm to 39.4 mm, with a standard deviation (10.6 mm) that was more than half of the mean value (17.9 mm); the mJSW was estimated to be between 0.53 mm and 1.29 mm, and had standard deviation (0.24 mm) that was just over a quarter of the mean (0.86 mm). Given the substantial standard deviations, it is clear that the range of R_e and mJSW was not generated by a few outliers. This range indicates a potentially high level of variability of thumb MCP joint congruence and minimal joint space width more widely: in small sample of 10 individuals, the largest value of R_e was over four times greater than the smallest, and the largest mJSW was over twice the smallest. Both the magnitude and variability of R_e observed (in this work) is within the range of previous joint congruence characterisations (Table 4).

Bone size did not play as strong a role (Fig. 7 and Fig. 8) in determining R_e and mJSW as one might expect—a larger joint could have a larger R_e and mJSW (with no change in shape) just by virtue of being bigger. There was little evidence of a positive correlation between the length of the first metacarpal and both R_e and mJSW. Similarly, the was no relationship evident in the ten joints between R_e and mJSW. However, studies have found fixed location and multiple location measures of joint space width to be superior to mJSW [45, 46]. Thus, it is possible this lack of correlation was due in part to the limitations of mJSW as a parameter.

4.4 Limitations

Although the number of participants is similar to several previous investigations of joint congruence [9, 12, 13], the small sample size limits how representative the results are and what can be said about thumb MCP joints more generally. In addition, like previous quantifications of joint congruence using CT imaging [15, 20], this study used the geometry of the subchondral bone as representative of articular surfaces of the joint. Thirdly, it was possible to use a flat elastic layer in the analogous FE simulations as the deformation required to make the layer conform between the bones was not substantial—the subchondral bone on the proximal end of the first proximal phalanx is relatively flat. If the methodology proposed in this work were extended to other diarthrodial joints where the articular surfaces are highly curved or irregular in shape, it is quite possible that the geometry of the elastic layer would need to be modified to more closely replicate those highly curved/irregular articular surfaces. This would avoid substantial strain generation not due to compression of the elastic layer.

The methodology currently requires the consistent identification of a longitudinal bone axis (the first proximal phalanx in this work), this may prove challenging in some diarthrodial joints *e.g.* bones in the foot and the knee, and thus further development of the methodology would be required. Additionally, by only using participants with healthy joint geometries, it was not possible to investigate whether localised geometric features resulting from osteoarthritis (for example) would be detectable with the methodology proposed here. It is quite possible that a step-change or non-linearity would occur (in the plot of P/E vs. ε^2_{min}) as the compressed area of the elastic layer increased beyond the bounds of a localised feature, which could provide useful clinical information about the joint. This would make an interesting future study. Finally, although the participant's hands were supported by a jig whilst CT scanned, some variation was observed in the relative position of the two bones connected at the thumb MCP joint. Previous investigations have had to face similar challenges and make assumptions regarding what is 'consistent' in the relative position of articular surfaces when quantifying joint congruence [9, 11]. Ideally, this methodology for quantifying joint congruence would be used in conjunction with a kinematic model for each joint—in addition to enabling variation in joint congruence with joint position be quantified, it would also ensure that the effect of variations in joint position on congruence would not be mistaken for differences in congruence between joints.

5 Conclusion

A new method for quantifying the congruence of diarthrodial joints has been proposed. It has been applied on 10 healthy thumb MCP joints. The quantification of congruence, the equivalent radius, is very closely-related to the 'congruence index' (CI) by Ateshain *et al.* [9], which can be approximated as its reciprocal. The ten thumb MCPs had similar levels of congruence and variability between participants as previous investigations. The minimal joint space width (in this joint position) could also be estimated in this new method. The principal advantage of the new method is its ability to quantify joint congruence directly from segmented CT or MRI scans. Previously, to evaluate the CI it has been necessary to identify the areas of the segmented bone surfaces that constitute the articular surfaces, carefully interpolate functions to describe the shape of these areas, and measure the relative orientation between each. This complexity is avoided in this new approach. It lends itself to ap-

plication in larger data sets and also in conjunction with kinematic models of joints, where the orientation of the bones is manipulated and this method used to assess congruence in different joint positions.

Acknowledgements

This research was conducted as part of the APRICOT project. The APRICOT project has received funding from the European Union's Horizon 2020 research and innovation programme under grant agreement No. 863183. This publication represents the views of the authors only. The European Commission is not responsible for any use that may be made of the information it contains.

The authors would like to thank Dr Andy Taylor (Aurora Medical Ltd., Chichester, UK) for helpful discussions regarding joint congruence. They would also like to thank Dr Kevin M. Moerman (National University of Ireland, Galway, Ireland) for helpful discussions regarding FE simulations in FEBio [38] and GIBBON [39].

References

[1] Clapham, C., and Nicholson, J., 2009. *The Concise Oxford Dictionary of Mathematics*. Oxford University Press.

[2] Buckwalter, J. A., Anderson, D. D., Brown, T. D., Tochigi, Y., and Martin, J. A., 2013. "The roles of mechanical stresses in the pathogenesis of osteoarthritis: Implications for treatment of joint injuries". *Cartilage,* **4**(4), pp. 286–294.

[3] Segal, N. A., Anderson, D. D., Iyer, K. S., Baker, J., Torner, J. C., Lynch, J. A., Felson, D. T., Lewis, C. E., and Brown, T. D., 2009. "Baseline articular contact stress levels predict incident symptomatic knee osteoarthritis development in the most cohort". *Journal of Orthopaedic Research,* **27**(12), pp. 1562–1568.

[4] Prendergast, P. J., and Lee, T. C., 2006. "Walking on water: The biomechanics of michael a. macconaill (1902–1987)". *Irish Journal of Medical Science,* **175**(3), pp. 69–75.

[5] MacConaill, M. A., 1932. "The function of intra-articular fibrocartilages, with special reference to the knee and inferior radio-ulnar joints". *Journal of anatomy,* **66**(Pt 2), pp. 210–227.

[6] Ateshian, G. A., and Mow, V. C., 2005. "Friction, lubrication, and wear of articular cartilage and diarthrodial joints". In *Basic Orthopaedic Biomechanics & Mechano-Biology*, V. C. Mow and R. Huiskes, eds. Lippincott Williams & Wilkins, Philadelphia, PA, USA, ch. 10, pp. 447–494.

[7] Ward, S. R., 2011. "Biomechanical applications to joint structure and function". In *Joint Structure and Function: A Comprehensive Analysis*, P. K. Levangie and C. C. Norkin, eds., 5 ed. F. A. Davis Company, Philadelphia, PA, USA, ch. 1, pp. 3–63.

[8] Kapandji, A. I., 2007. *The Physiology of the Joints: Volume 1, The Upper Limb*, 6 ed. Churchill Livingstone.

[9] Ateshian, G., Rosenwasser, M., and Mow, V., 1992. "Curvature characteristics and congruence of the thumb carpometacarpal joint: Differences between female and male joints". *Journal of Biomechanics,* **25**(6), pp. 591–607.

[10] Johnson, K., 1985. *Contact Mechanics*. Cambridge University Press.

[11] Xu, L., Strauch, R. J., Ateshian, G. A., Pawluk, R. J., Mow, V. C., and Rosenwasser, M. P., 1998. "Topography of the osteoarthritic thumb carpometacarpal joint and its variations with regard to gender, age, site, and osteoarthritic stage". *The Journal of Hand Surgery,* **23**(3), pp. 454–464.

[12] Hohe, J., Ateshian, G., Reiser, M., Englmeier, K.-H., and Eckstein, F., 2002. "Surface size, curvature analysis, and assessment of knee joint incongruity with mri in vivo". *Magnetic Resonance in Medicine,* **47**(3), pp. 554–561.

[13] Connolly, K. D., Ronsky, J. L., Westover, L. M., Küpper, J. C., and Frayne, R., 2009. "Analysis Techniques for Congruence of the Patellofemoral Joint". *Journal of Biomechanical Engineering,* **131**(12), 11. 124503.

[14] Tummala, S., Nielsen, M., Lillholm, M., Christiansen, C., and Dam, E. B., 2012. "Automatic quantification of tibio-femoral contact area and congruity". *IEEE Transactions on Medical Imaging,* **31**(7), pp. 1404–1412.

[15] Halilaj, E., Laidlaw, D. H., Moore, D. C., and Crisco, J. J., 2014. "Polar Histograms of Curvature for Quantifying Skeletal Joint Shape and Congruence". *Journal of Biomechanical Engineering,* **136**(9), 07. 094503.

[16] Conconi, M., and Castelli, V. P., 2014. "A sound and efficient measure of joint congruence". *Proceedings of the Institution of Mechanical Engineers, Part H: Journal of Engineering in Medicine,* **228**(9), pp. 935–941.

[17] Zuiderbaan, H. A., Khamaisy, S., Thein, R., Nawabi, D. H., and Pearle, A. D., 2015. "Congruence and joint space width alterations of the medial compartment following lateral unicompartmental knee arthroplasty". *The Bone & Joint Journal,* **97-B**(1), pp. 50–55.

[18] Charbonnier, C., Kolo, F. C., Duthon, V. B., Magnenat-Thalmann, N., Becker, C. D., Hoffmeyer, P., and Menetrey, J., 2011. "Assessment of congruence and impingement of the hip joint in professional ballet dancers: A motion capture study". *The American Journal of Sports Medicine,* **39**(3), pp. 557–566.

[19] von Eisenhart, R., Adam, C., Steinlechner, M., Müller-Gerbl, M., and Eckstein, F., 1999. "Quantitative determination of joint incongruity and pressure distribution during simulated gait and cartilage thickness in the human hip joint". *Journal of Orthopaedic Research,* **17**(4), pp. 532–539.

[20] Conconi, M., Halilaj, E., Parenti Castelli, V., and

Crisco, J. J., 2014. "Is early osteoarthritis associated with differences in joint congruence?". *Journal of Biomechanics,* **47**(16), pp. 3787–3793.

[21] Cooney 3rd, W., and Chao, E., 1977. "Biomechanical analysis of static forces in the thumb during hand function". *The Journal of Bone and Joint Surgery,* **59**(1), pp. 27–36.

[22] Hollister, A., Giurintano, D. J., Buford, W. L., Myers, L. M., and Novick, A., 1995. "The axes of rotation of the thumb interphalangeal and metacarpophalangeal joints". *Clinical Orthopaedics and Related Research,* **320**, pp. 188–193.

[23] Harris, H., and Joseph, J., 1949. "Variation in extension of the metacarpo-phalangeal and interphalangeal joints of the thumb". *The Journal of Bone and Joint Surgery. British volume,* **31-B**(4), pp. 547–559.

[24] Joseph, J., 1951. "Further studies of the metacarpophalangeal and interphalangeal joints of the thumb". *Journal of anatomy,* **85**(3), pp. 221–229.

[25] Yoshida, R., House, H. O., Patterson, R. M., Shah, M. A., and Viegas, S. F., 2003. "Motion and morphology of the thumb metacarpophalangeal joint". *The Journal of Hand Surgery,* **28**(5), pp. 753–757.

[26] Metcalf, C. D., Phillips, C., Forrester, A., Glodowski, J., Simpson, K., Everitt, C., Darekar, A., King, L., Warwick, D., and Dickinson, A. S., 2020. "Quantifying soft tissue artefacts and imaging variability in motion capture of the fingers". *Annals of Biomedical Engineering,* **48**(5), pp. 1551–1561.

[27] MATLAB, 2020. *9.7.0.1296695 (R2019b)*. The MathWorks Inc., Natick, Massachusetts.

[28] Wu, G., van der Helm, F. C., (DirkJan) Veeger, H., Makhsous, M., Van Roy, P., Anglin, C., Nagels, J., Karduna, A. R., McQuade, K., Wang, X., Werner, F. W., and Buchholz, B., 2005. "Isb recommendation on definitions of joint coordinate systems of various joints for the reporting of human joint motion—part ii: shoulder, elbow, wrist and hand". *Journal of Biomechanics,* **38**(5), pp. 981–992.

[29] Ryu, J. H., Miyata, N., Kouchi, M., Mochimaru, M., and Lee, K. H., 2006. "Analysis of skin movement with respect to flexional bone motion using mr images of a hand". *Journal of Biomechanics,* **39**(5), pp. 844–852.

[30] Besl, P., and McKay, N. D., 1992. "A method for registration of 3-d shapes". *IEEE Transactions on Pattern Analysis and Machine Intelligence,* **14**(2), pp. 239–256.

[31] Wilm, J., 2021. Iterative closest point. `https://www.mathworks.com/matlabcentral/fileexchange/27804-iterative-closest-point`. Retrieved: 2021-08-06.

[32] Fregly, B. J., Bei, Y., and Sylvester, M. E., 2003. "Experimental evaluation of an elastic foundation model to predict contact pressures in knee replacements". *Journal of Biomechanics,* **36**(11), pp. 1659–1668.

[33] Henak, C. R., Anderson, A. E., and Weiss, J. A., 2013. "Subject-Specific Analysis of Joint Contact Mechanics: Application to the Study of Osteoarthritis and Surgical Planning". *Journal of Biomechanical Engineering,* **135**(2), 02. 021003.

[34] Li, G., Sakamoto, M., and Chao, E. Y., 1997. "A comparison of different methods in predicting static pressure distribution in articulating joints". *Journal of Biomechanics,* **30**(6), pp. 635–638.

[35] Blankevoort, L., Kuiper, J., Huiskes, R., and Grootenboer, H., 1991. "Articular contact in a three-dimensional model of the knee". *Journal of Biomechanics,* **24**(11), pp. 1019–1031.

[36] Ateshian, G. A., Henak, C. R., and Weiss, J. A., 2015. "Toward patient-specific articular contact mechanics". *Journal of Biomechanics,* **48**(5), pp. 779–786.

[37] HYDE, S., NINHAM, B. W., ANDERSSON, S., LARSSON, K., LANDH, T., BLUM, Z., and LIDIN, S., 1997. "Chapter 1 - the mathematics of curvature". In *The Language of Shape*, S. HYDE, B. W. NINHAM, S. ANDERSSON, K. LARSSON, T. LANDH, Z. BLUM, and S. LIDIN, eds. Elsevier Science B.V., Amsterdam, pp. 1–42.

[38] Maas, S. A., Ellis, B. J., Ateshian, G. A., and Weiss, J. A., 2012. "FEBio: Finite Elements for Biomechanics". *Journal of Biomechanical Engineering,* **134**(1).

[39] Moerman, K. M., 2018. "Gibbon: The geometry and image-based bioengineering add-on". *Journal of Open Source Software,* **3**(22), p. 506.

[40] FEBio. Febio software suite: Journal articles. `https://febio.org/publications/journal-articles/`. Accessed: 2021-04-13.

[41] Maas, S. A., Weiss, J. A., and Ateshian, G. A., 2021. FEBio User's Manual: Version 3.4. `https://help.febio.org/FebioUser/FEBio_um_3-4.html`.

[42] Laursen, T. A., and Maker, B. N., 1995. "An augmented lagrangian quasi-newton solver for constrained nonlinear finite element applications". *International Journal for Numerical Methods in Engineering,* **38**(21), pp. 3571–3590.

[43] Moran, J. M., Hemann, J. H., and Greenwald, A. S., 1985. "Finger joint contact areas and pressures". *Journal of Orthopaedic Research,* **3**(1), pp. 49–55.

[44] Bhatia, R., and Kittaneh, F., 2000. "Notes on matrix arithmetic–geometric mean inequalities". *Linear Algebra and its Applications,* **308**(1), pp. 203–211.

[45] Roth, M., Wirth, W., Emmanuel, K., Culvenor, A. G., and Eckstein, F., 2017. "The contribution of 3d quantitative meniscal and cartilage measures to variation in normal radiographic joint space width—data from the osteoarthritis initiative healthy reference cohort". *European Journal of Radiology,* **87**, pp. 90–98.

[46] Cheung, J. C.-W., Tam, A. Y.-C., Chan, L.-C., Chan, P.-K., and Wen, C., 2021. "Superiority of multiple-joint space width over minimum-joint space width approach in the machine learning for radiographic severity and knee osteoarthritis progression". *Biology,* **10**(11).